

# Thermal post buckling analysis of smart SMA hybrid sandwich composite plate

Polymers and Polymer Composites  
2021, Vol. 29(9S) S344–S360  
© The Author(s) 2021  
Article reuse guidelines:  
sagepub.com/journals-permissions  
DOI: 10.1177/09673911211001276  
journals.sagepub.com/home/ppc



Achchhe Lal  and Kanif Markad

## Abstract

Thermal post-buckling analysis of smart sandwich plates has been presented with the incorporation of shape memory alloy (SMA) and shape memory polymer (SMP) in laminated composite structure under uniform temperature distribution. Buckling analysis is based on higher order shear deformation theory (HSDT) with von Karman nonlinearity by finite element method (FEM). Evaluation of critical buckling temperature has been performed under the action of inplane uniform temperature distribution for different boundary conditions, plate's aspect and thickness ratio, modulus ratio, ply orientations of smart SMA hybrid sandwich composite plate. Shape memory alloys itself acting uniquely under temperature variation and with SMA reinforced SMP laminated composite plate this phenomenon extended further under dynamic temperature condition for thermal buckling behavior. Also SMA with different strain rate and variation in SMA volume fraction is also presented to understand the cumulative buckling behavior.

## Keywords

Laminated sandwich composite plates (LCP), shape memory alloy (SMA), shape memory polymer composite (SMPC), HSDT, SMP

Received 23 October 2020; accepted 10 February 2021

## 1. Introduction

Smart materials have the characteristics to memorize a stimuli such as temperature, electric or magnetic field and correspondingly change its shape, natural frequency, stiffness, buckling, hardness and other mechanical properties. Shape memory alloys (SMA) are one of such class of smart material, which has the capability to regain its original shape/form from a deformation, when heated at an elevated temperature.<sup>1</sup> As compared to other smart materials, SMA has the highest recovery strain field and flexibility, due to its distinct thermo-mechanical, shape memory and pseudo-elastic properties toward the deviations in load, temperature and stresses.<sup>2</sup> Moreover, it has some other significant properties of high damping capacity, recovery stresses and superelasticity, these salient features which simplifies the complexity of standard technology, makes SMA even more appealing for sophisticated applications in aerospace, spacecraft, micro-electromechanical systems (MEMS) and other intelligent systems.<sup>3</sup>


In the recent decades, laminated composites have found an increasing applications in various engineering structures due to its high strength to weight ratio and stiffness. Components of aircrafts, missiles and space vehicles are extensively being developed from these composites. One of the most common problems faced, with these application, includes volatility in the ambience of thermal load. As a result, researchers have come up with the reinforcement of SMA wires in the laminates as a viable solution to resist mechanical, thermal or thermo-mechanical loads. Moreover, focus has also been on the sandwich structures because of its discrete features, in aerospace, civil, electronics, transportation and marine in previous decades. Sandwich panels consist of a pair of thin sheets, which may be made from metals, laminates of functionally grade material (FGM), encompassing a low density and weight material such as polymer foam of honeycomb structure.<sup>4–7</sup> Embedded smart material in the structure has significantly enhance the structural integrity with improved resistance to vibration and buckling.

Mechanical Engineering Department, SVNIT, Surat, India

## Corresponding author:

Achchhe Lal, Mechanical Engineering Department, SVNIT, Surat 395007, India.  
Email: lalachchhe@yahoo.co.in



  
PRINCIPAL  
Dr Vithalrao Vikhe Patil  
College of Engineering  
Ahmednagar

Buckling and post-buckling analysis of composite beam, plates and shells has been taken into consideration by researchers, which affects stability of the structures in thermal environment.<sup>8,9</sup> Embedding SMA, such as Nitinol wires, in the structure has satisfactorily enhanced the thermal buckling resistance, particularly in composites and sandwich panel subjected to thermal environment.<sup>10–12</sup> When SMA wire reinforced composites are subjected to high temperature surplus strains are recovered, which induces internal tensions. This process create tension in structure and improves its thermal buckling and post buckling resistivity, and provide hindrance to the resonance in the structure. There are few articles that deals with thermal buckling of composites or sandwich panels, which provides an opportunity to the authors to analyze the phenomenon in the current work.

Some relevant work of thermal buckling of composites panel are discussed prior to the focus on SMA reinforcement for the sake of continuity. Girish and Ramachandra<sup>13</sup> presented the buckling analysis for the composite plates developed from higher order shear deformation theory (HSDT) with von Karman kinematics. Singh et al.<sup>14</sup> analyzed free vibrations of laminated plates with high amplitude vibration using nonlinear von Karman geometric model. Nonlinear response of an anisotropic laminated composites was evaluated by Reddy and Chao<sup>15</sup> with consideration of von Karman nonlinearity based on first order shear deformation theory FSDT. Khdeir<sup>16</sup> performed analysis of thermally buckled analysis of laminated composites with various orientations and presented comparison of various beam theories, for instance Classical Beam Theory, FSDT and HSDT. Considering 3 degree of freedom (DOF) shear deformation beam theory, Aydogdu<sup>17</sup> evaluated amplitude of thermal buckling in composites beam. Vosoughi et al.<sup>18</sup> also presented post-buckling phenomenon of thermally buckled laminated composite beams using FSDT with the implementation of numerical GDQ algorithm.

SMA has been embedded in the sandwich/composite structures to harness the buckling resistance property of pre-strained SMA. Initial works mainly focused on the incorporation of SMA wire in various volume fractions to control buckling of the composites. Rogers and Bakers<sup>19</sup> utilized SMA wires in graphite reinforced epoxy composites to enhance in its natural frequency and control its vibration. Baz et al.<sup>20</sup> studied the control of SMA wires on the vibration and buckling behavior on composites. Khalili and Akbari<sup>21</sup> performed experimental critical buckling load evaluation of SMA embedded in composite panel under different stacking sequence and boundary conditions and concluded effectiveness of SMA incorporation than any other parameter. Choi et al.<sup>22</sup> also experimentally analyzed the performance of SMA fibers on the active buckling control nature which showed positive results. Moreover, Birman<sup>23</sup> studied buckling behavior of sandwich plates incorporated with functionally graded SMA under influence of uniform temperature rise and uniaxial compression.

Computational estimation of post-buckling analysis is helpful to design the composites/sandwich structures with better reliability and opening new avenues to explore possibilities to resist buckling subjected to thermal loading. Lee et al.<sup>24</sup> presented numerical simulation of the buckling performance of laminated composite shells embedded with SMA fibers under thermal loading. Investigation presented the effects of SMA fiber reinforcements on the characteristics of thermal buckling through numerical analysis in ABAQUS. Park et al.<sup>25</sup> studied the effects of embedding SMA fibers on the vibration property of the composites, subjected to thermal buckling through FSDT. The results were encouraging with increase in the buckling temperature and resultant deflection due to the application of thermal load. Li et al.<sup>26</sup> evaluated free vibration of thermally buckled aluminium plate reinforced with SMA wire based on Brinson's model, which estimated in the enhancement of the buckling resistance due to thermal loading. Shiau et al.<sup>27</sup> inspected the influence of SMA fiber spacing on vibration of different ply orientation under the influence of buckling based on HSDT and principle of virtual work with von-Karman nonlinearity. Parhi and Singh<sup>28</sup> calculated the nonlinear free vibration response of composite with SMA hybridization for spherical and cylindrical composite shell panels. Nejati et al.<sup>29</sup> also performed the non-linear free vibration analysis of double curved sandwich panels, based on HSDT with von Karman geometric nonlinearity through Hamilton principle, embedded with pre-strained SMA fibers subjected to thermal buckling. Recovery stresses of SMA fibers were simulated by one-dimensional Brinson model and incorporated in the sandwich to estimate natural frequency and threshold buckling temperature. Embedding of SMA wires in the composite sandwich estimated to increase natural frequencies and subsequently increase resistance to thermal buckling. Salim et al.<sup>30</sup> employed Brinson's model to simulate SMA's thermomechanical behavior with incorporation of genetic algorithm to optimize SMA fiber orientation to maximize natural frequency of laminated composite thermal environment. This presented the stacking sequence with the maximum natural frequency during vibration under thermal loading.

Panda and Singh<sup>31,32</sup> analyzed the buckling nature of laminated composite panel with and without SMA wire reinforcements through the HSDT taking Green–Lagrange nonlinearity. Xia and Shen<sup>33</sup> presented buckling and post-buckling amplitudes of FGM with piezoelectric actuators in a thermal environment based on nonlinear von Karman HSDT. Tawfik et al.<sup>34</sup> analyzed SMA fibers reinforced laminated panels under the influence of combined aerodynamic and thermal loading through nonlinear FEM based on the von Karman relations. LCP embedded with SMA analyzed for buckling behavior and also concluded the buckling resistance improvement with the utilization of SMA.<sup>35–37</sup> Samadpour et al.<sup>38</sup> predicted the nonlinear vibration behavior to estimate critical buckling temperature (CBT) and natural frequency of composite plates embedded with SMA wires. The analysis was based on FSDT with the consideration of von Karman kinematics and Hamilton principle, and 1D Brinson constitutive model was employed to simulate shape memory effect in SMA. Bayat and Ekhteraei Toussi<sup>39</sup> also presented the thermomechanical behavior of SMA reinforced composite plates

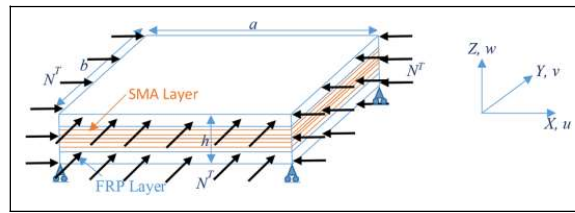


**Figure 1.** Geometry of smart sandwich composite plate.

based on one-dimensional Brinson model in thermal environment. Governing equations were developed using Layer-Wise Theory (LWT) of beam along with von Karman relations, to obtain closed form solutions of nonlinear equations.

Asadi et al.<sup>40</sup> analyzed the temperature based constancy of SMA fiber reinforced layered composites through HSDT and calculated closed-form solution to determine load deflection profile for simply supported condition. Kabir and Tehrani<sup>41</sup> also presented a closed form solution for buckling analysis under thermomechanical loading for a symmetric LCP embedded with SMA wires using nonlinear von Karman sense FSDT. The effect of SMA behavior considering one dimensional Brinson model was more effectively captured with Active strain energy tuning (ASET) than the active property tuning (APT) method. Karimiasl et al.<sup>42</sup> performed numerical analysis of buckling phenomenon of hygro-thermally buckled doubly curved composite shells reinforced with SMA wires using Halpin-Tsai model. Analysis was based on third order shear deformation theory (TSDT) with consideration of von Kármán-Donnell geometric nonlinearity.

From the available literatures it is evident that, there is an opportunity to study post buckling analysis of laminated sandwich composite plate and SMA embedded sandwich composite plate for estimating its resistance against buckling, under different boundary conditions (BC), temperature variations, SMA volume fraction variation, plate aspect and thickness ratio along with the number of layers. Literature survey also revealed that, effect of temperature variation over shape memory polymer composite (SMPC) embedded with SMA, has not been performed with the current method.

Present study clearly analyzes the post-buckling performance of the laminated composite plate (LCP) and SMA embedded sandwich composite plate. For the analysis, effective HSDT with von-Karman nonlinearity is implemented with finite element method (FEM). Study includes the effect of variation of number of layers, its orientations, modulus ratio, plate's aspect and thickness ratio, temperature variation, amplitude ratio, number of SMA layer along with its volume fraction and percentage strain rate variation imposed on SMA. Various modes of buckling under different boundary conditions are presented for better elaboration of the buckling phenomenon. Study also evaluate the effect of shape memory polymers on buckling behavior of SMA hybrid composite under glass transition region and SMA volume fraction variation.

## 2. General mathematical formulation

The post-buckling analysis of smart sandwich composite plate using HSDT with von-Karman nonlinear kinematics FEM is presented with the programming in MATLAB environment. Using  $C^0$  continuity, seven degrees of freedom (DOF), nine noded elemental model prepared with FEM which is utilized for the evaluation of the critical buckling temperature of the smart sandwich composite plate. For the FEM analysis the smart sandwich composite plate is used which is shown in Figure 1. The plate is having length ' $a$ ', width ' $b$ ' and thickness ' $h$ ' which is assumed uniform throughout the analysis until stated.

### 2.1. Material properties of SMP matrix

Shape memory polymer (SMP) is a category of smart materials, utilized in the current study as a temperature sensitive and have corresponding dynamic mechanical properties governed by glass transition temperature ( $T_g$ ) of polymers. Temperature dependent elastic moduli can be experimentally investigated from Dynamic Mechanical Analysis (DMA) or can derived from curve-fitting of experimental results. Mathematical relation proposed by Mahieux and Reifsnider,<sup>43</sup> has been adopted to simulate DMA results of across glass transition region of SMP at uniform frequency, stated in Eq. (1).<sup>44</sup> Storage modulus of the material obtained from DMA, has been considered as modulus of SMP, as the loss modulus is negligible compared to storage modulus.<sup>45</sup>

$$E_m(T) = (E_1 - E_2) \cdot \exp\left(-\left(\frac{T}{T_\beta}\right)^{m1}\right) + (E_2 - E_3) \cdot \exp\left(-\left(\frac{T}{T_g}\right)^{m2}\right) + E_3 \cdot \exp\left(-\left(\frac{T}{T_f}\right)^{m3}\right) \quad (1)$$

Where,  $E_1$ ,  $E_2$  and  $E_3$  are material's moduli at the initiation of  $\beta$ -transition, glass transition and flow region respectively with corresponding values are 2552 MPa, 1876 MPa and 5 MPa respectively.  $T$  is considered range of temperature encompassing  $T_\beta = 22.2^\circ\text{C}$ ,  $T_g = 32^\circ\text{C}$  and  $T_f = 142.5^\circ\text{C}$ , which indicate temperature at the start of  $\beta$ -transition, glass

transition and flow region respectively.  $m_1$ ,  $m_2$  and  $m_3$  are Weibull exponents with values of 19.3, 58.4, 177.6 respectively as per Gu et al.<sup>45</sup> Poissons ratio with respect to temperature is evaluated by Eq. (2) and Eq. (3), Qi et al.<sup>46</sup>

$$\mu = \mu_g \nu_g + \mu_r (1 - \nu_g) \quad (2)$$

$$\nu_g = 1 - \frac{1}{1 + \exp[-(T - T_m)/z]} \quad (3)$$

Where  $\mu_g$  and  $\mu_r$  are Poisson's ratio of the frozen phase and active phase respectively with values of 0.35 and 0.499 respectively.  $\nu_g$  is the frozen phase volume fraction, calculated by Eq. (3).  $T_m$  is reference temperature considered as 27.5°C.  $Z = 7$  is the width of the phase transition zone. The values of SMP composite properties in series and parallel are estimated from the theory of volume averaging by Gu et al.<sup>45</sup> Similarly, the material properties of overall SMA embedded SMP sandwich composite are evaluated as,

$$\begin{aligned} E_1 &= E_{c1}V_m + E_sV_s; \quad E_2 = (E_sE_{c2})/(E_{c2}V_s + E_sV_m); \quad G_{12} = (G_sG_{c12})/(G_{c12}V_s + G_sV_m); \quad G_{13} = G_{c12}; \\ G_{23} &= (G_{c23}V_m + G_sV_s); \quad V_{12} = V_{c12}V_m + v_sV_s; \quad V_{21} = V_{12}(E_2/E_1); \\ \alpha_1 &= (E_{c1}\alpha_{c1}V_m + E_s\alpha_sV_s)/E_1; \quad \alpha_2 = (\alpha_{c2}V_m + \alpha_sV_s); \quad \alpha_{12} = 0; \quad \rho = \rho_mV_m + \rho_sV_s; \end{aligned} \quad (4)$$

In Eq. (4) the unknown composite matrix material property evaluated as,

$$E_{c1} = E_{f1}\nu_f + E_m\nu_m \quad (5)$$

$$E_{c2} = (1 - C)E_{c2}^1 + CE_{c2}^2 \quad (6)$$

$$\mu_{c21} = (1 - C)\mu_{c21}^1 + C\mu_{c21}^2 \quad (7)$$

$$\mu_{c12} = \mu_{c21} \frac{E_{c2}}{E_{c1}} \quad (8)$$

$$G_{c12} = (1 - C)G_{c12}^1 + CG_{c12}^2 \quad (9)$$

Where  $E_{c1}$  and  $E_{c2}$  are modulus of composites along longitudinal and transverse directions respectively.  $E_{f1} = 2.3 \times 10^6 \text{ MPa}$  and  $E_{f2} = 8.2 \times 10^3 \text{ MPa}$  are Young's modulus of fiber along longitudinal and transverse directions respectively.  $G_{f12} = 2.73 \times 10^4 \text{ MPa}$  is shear modulus along plane 1–2.  $G_{c12}$  is shear modulus of composite in 1–2 plane.  $C = 0.2$  is transverse contact coefficient between fibers.  $\mu_f = 0.25$  is Poisson's ratio of carbon fiber.  $\mu_{c12}$  and  $\mu_{c21}$  indicate Poisson's ratio of composites along 1–2 and 2–1 plane respectively. The values of properties in series and parallel are estimated from the following equations, which will be substituted in Eqs. (5) to (9). The values of related individual parameters are taken from Gu et al.<sup>45</sup>

$$E_{c2}^1 = \frac{E_{f2}E_m}{E_{f2}\nu_m + E_m\nu_f} \quad (10)$$

$$E_{c2}^2 = E_{f2}\nu_f + E_m\nu_m \quad (11)$$

$$\mu_{c21}^1 = \mu_f\nu_f + \mu_m\nu_m \quad (12)$$

$$\mu_{c21}^2 = \frac{\mu_f E_{f2}\nu_f + \mu_m E_m\nu_m}{E_{f2}\nu_f + E_m\nu_m} \quad (13)$$

$$G_{c12}^1 = \frac{G_{f12}G_m}{E_{f12}\nu_m + G_m\nu_f} \quad (14)$$

$$G_{c12}^2 = G_{f12}\nu_f + G_m\nu_m \quad (15)$$

## 2.2. Displacement field equation

The suitable streamlined form of the displacement field can be written as, Jagtap et al.<sup>47</sup>

$$\begin{aligned} U &= u(x, y) + g_1(z)\phi_x(x, y) + g_2(z)\Phi_x(x, y) \\ V &= v(x, y) + g_1(z)\phi_y(x, y) + g_2(z)\Phi_y(x, y) \\ W &= w(x, y) \end{aligned} \quad (16)$$

In this equation slopes in x and y directions represented as,

$$\Phi_x = \frac{\partial w}{\partial x}, \quad \Phi_y = \frac{\partial w}{\partial y}, \quad g_1(z) = 1 * z - (4/3h_2)z^3 \quad \text{and} \quad g_2(z) = -(4/3h_2)z^3 \quad (17)$$

### 2.3. Relation between strain and displacement

With the slight deformation assumption, linear strain in laminas are represented as,

$$\begin{Bmatrix} \varepsilon_x \\ \varepsilon_y \\ \varepsilon_z \\ \gamma_{xy} \\ \gamma_{xz} \\ \gamma_{yz} \end{Bmatrix} = \begin{Bmatrix} \partial u / \partial x \\ \partial v / \partial y \\ 0 \\ \partial u / \partial x + \partial v / \partial y \\ \partial u / \partial z + \partial w / \partial x \\ \partial v / \partial z + \partial w / \partial y \end{Bmatrix} \quad (18)$$

Corresponding to displacement fields, strain vectors presented as

$$\begin{aligned} \{\bar{\varepsilon}\} &= \{\varepsilon_x, \varepsilon_y, \gamma_{xy}, \gamma_{xz}, \gamma_{yz}\}^T \\ \{\bar{\varepsilon}\} &= \{\mathbf{e}_l\} - \{\mathbf{e}_{nl}\} - \{\mathbf{e}_t\} \\ \{\mathbf{e}_t\} &= \{\alpha_1 \Delta T \quad \alpha_2 \Delta T \quad 0 \quad 0 \quad 0\} \end{aligned} \quad (19)$$

Midplane strain vectors and displacement vector can be written as,

$$\{\bar{\varepsilon}\} = (\varepsilon_1^0 \quad \varepsilon_2^0 \quad \varepsilon_6^0 \quad k_1^0 \quad k_2^0 \quad k_6^0 \quad k_1^2 \quad k_2^2 \quad k_6^2 \quad \varepsilon_4^0 \quad \varepsilon_5^0 \quad k_4^2 \quad k_5^2) \quad (20)$$

$$q = (u \quad v \quad w \quad \Phi_y \quad \Phi_x \quad \phi_y \quad \phi_x) \quad (21)$$

The linear strain vector can be written as,  $\{\varepsilon_l\} = [L]\{q\}$  and  $[L]$  is defined in (A1).

The nonlinear strain vector can be inscribed as, Lal et al.<sup>48</sup>

$$\{\varepsilon_{nl}\} = \frac{1}{2} [A] \{\phi\} \quad (22)$$

$$\text{Where, } [A] = \begin{bmatrix} \frac{\partial w}{\partial x} & 0 & \frac{\partial w}{\partial y} & 0 & 0 \\ 0 & \frac{\partial w}{\partial x} & \frac{\partial w}{\partial y} & 0 & 0 \end{bmatrix}^T, \quad \phi = \frac{1}{2} \begin{bmatrix} \frac{\partial w}{\partial x} \\ \frac{\partial w}{\partial y} \end{bmatrix} \quad (23)$$

### 2.4. Relation between strain and stress

The elastic constitutive relations for three mutually orthogonal planes of material symmetry exist subjected to uniform temperature and  $\sigma_z = 0$  the relation between strain and stress for SMA embedded composite of kth layer with reference to reference coordinate system by following relation, Kumar and Singh<sup>49</sup>

$$\{\sigma\}^k = [\bar{Q}]^k \{\bar{\varepsilon}\}^k + \{\sigma_r\}^k V_s - ([\bar{Q}]_m \{\alpha\}_m V_m)^k \Delta T \quad (24)$$

Here  $[\bar{Q}]^k$  and  $[\bar{Q}]_m$  are the reduced transferred stiffness matrix of smart composite plate and composite matrix respectively and given in (A2).  $\{\sigma_r\}$  is the recovery stress generated in SMA due to temperature variation  $\Delta T$  as shown in Figure 1.6 from Tawfik.<sup>50</sup>  $V_s$  and  $V_m$  are the volume fraction of SMA and matrix respectively.

### 2.5. Finite element modeling

To analyze the presented model using FEM, the element geometry and displacement vector can be represented as follows, Lal et al.<sup>48</sup>

$$\{q\}^e = \sum_{i=1}^{NN} N_i^e \{q_i\}^e, \quad x = \sum_{i=1}^{NN} N_i \{x_i\}, \quad y = \sum_{i=1}^{NN} N_i \{y_i\} \quad (25)$$

Here, total nodes per element is defined by  $NN$  and  $N$  defines the shape function for  $i^{th}$  node.  $x_i$  and  $y_i$  are Cartesian coordinate for  $i^{th}$  node.

Using  $[B_i]$  for  $i$ th node and differential operator  $[L]$ , relationship between strain-displacement defined as,  $[B_i] = [L]N_i$

## 2.6. Strain energy in composite plate

Total strain energy in the composite plate is the combination of linear and nonlinear strain energy combination and it is represented as,

$$\Pi_1 = \frac{1}{2} \sum_{i=1}^{NE} [q^{eT} (k_l + k_{nl}) q^e] = \{q\}^T [K_l + K_{nl}] \{q\} \quad (26)$$

$NE$  and  $i$  are the number of elements and elemental, respectively and  $q$  is the global displacement vector. In natural coordinate system  $(Z, \eta)$ , elemental stiffness matrix defined as,

$$[k_l^e] = \int_{-1}^1 \int_{-1}^1 [B]^T [D] [B] \det[J] d\xi d\eta \quad (27)$$

$$\text{Where the Jacobean } [J] \text{ is, } [J] = \begin{bmatrix} \frac{dx}{d\xi} & \frac{dy}{d\xi} \\ \frac{dx}{d\eta} & \frac{dy}{d\eta} \end{bmatrix} \quad (28)$$

$$\begin{aligned} k_{nl1}^e &= \frac{1}{2} \int_{A^{(e)}} B_\phi^{eT} (D_1) \{A^e\} \{G^e\} dx dy; \\ k_{nl2}^e &= \frac{1}{2} \int_{A^{(e)}} \{G^e\}^T \{A^e\}^T (D_2) \{B\}^e dx dy; \\ k_{nl3}^e &= \frac{1}{2} \int_{A^{(e)}} \{G^e\}^T \{A^e\}^T (D_3) \{A^e\} \{G^e\} dx dy \\ K_{nl}^e &= \frac{1}{2} \sum_{i=1}^{NE} [k_{nl1}^e + k_{nl2}^e + k_{nl3}^e] \end{aligned} \quad (29)$$

In this equation  $D_1, D_2, D_3$  are the elastic stiffness matrices of the composite plate respectively and shown in (A3) and (A4).

## 2.7. Work done and strain energy due to thermal loading

Due to thermal load application, the work potential stored can be given as,

$$\begin{aligned} N_T &= \sum_{k=1}^{NL} \int_{z_{k-1}}^{z_k} [\overline{Q}] \{\varepsilon_t\} dz; & N_M &= \sum_{k=1}^{NL} \int_{z_{k-1}}^{z_k} [\overline{Q}] \{\varepsilon_t\} z dz; & N_P &= \sum_{k=1}^{NL} \int_{z_{k-1}}^{z_k} [\overline{Q}] \{\varepsilon_t\} z^3 dz \\ N_O^T &= N_T + N_M + N_P \end{aligned} \quad (30)$$

Where  $N_O^T$  is the final thermal compressive load acting over the plate.

$$\begin{aligned} \Pi_2 &= \frac{1}{2} \sum_{i=1}^{NE} [q^{eT} \lambda [K_g] q^e] = \lambda \{q^T\} [K_g] \{q\} \\ \text{Where,} & \\ [K_g] &= \frac{1}{2} \int_A B_G^{eT} N_O^T B_G^e \end{aligned} \quad (31)$$

## 2.8. Governing equation

The equilibrium equation governing the present problem for the laminate can be obtained by minimizing the total potential energy with respect to generalized displacements  $(\partial(\Pi_1 - \Pi_2)/\partial q = 0)$ ,

$$\begin{aligned} [K - \lambda K_g] \{q_i\} &= 0 \\ [K] \{q\} &= \lambda [K_g] \{q\} \\ \text{Where, } [K] &= [K_l] + [K_{nl}] \text{ with } [K_{nl}] = [K_{nl1}] + [K_{nl2}] + [K_{nl3}] \end{aligned} \quad (32)$$



**Table 1.** Convergence study of FE solution for various mesh size.

Number of element (nel)	45/0/0/45		45/–45/45/–45/45/–45	
	a/h = 50	a/h = 100	a/h = 50	a/h = 100
3 × 3	0.650	0.187	0.668	0.180
4 × 4	0.518	0.157	0.594	0.158
5 × 5	0.516	0.155	0.566	0.159
6 × 6	0.515	0.156	0.596	0.166

**Table 2.** Validation and variation of NCBT with plate aspect ratio.

Layer	a/h	Matsunaga et al. <sup>51</sup>	Noor and Burton <sup>52</sup>	Singh et al. <sup>53</sup>	Mirzaei and Kiani <sup>54</sup>	Present
[0/90/0]	10	0.07467	—	—	—	0.0771
	20	0.02291	0.02308	0.02308	0.02346	0.02298
	100	0.000991	0.000996	0.0009917	0.000992	0.00106
[0/90]	10	0.04323	—	—	—	0.0784
	20	0.01178	—	—	—	0.0261
	100	0.0004857	—	—	—	0.00122
[0]	10	0.05782	—	—	—	0.05469
	20	0.01739	0.01771	0.01752	0.01739	0.01731
	100	0.0007463	0.0007463	0.0007463	0.0007469	0.000758

The Eq. (32) is nonlinear buckling equation which is evaluated and solved as eigenvalue problem. In the expression  $\lambda = \Delta T_{cr}$ , is the critical buckling temperature.

### 3. Results and discussion

Present thermal buckling analysis of composite panel/plate is divided in three sections. In the first section, convergence and validation study is performed to present effectiveness and accuracy of the user-defined MATLAB program. In the second section, thermal buckling analysis of laminated composite plate is carried out. Thermal buckling analysis of smart sandwich composite plate is performed in the third section. Under the study, various boundary conditions (BC) are implemented which are indicated as,

$$SSSS-I: u = v = w = \theta_x = \phi_x = 0 \text{ at } y = 0 \text{ and } b \quad SSSS-II: u = w = \theta_x = \phi_x = 0 \text{ at } y = 0 \text{ and } b \\ u = v = w = \theta_y = \phi_y = 0 \text{ at } x = 0 \text{ and } a \quad u = v = w = \theta_y = \phi_y = 0 \text{ at } x = 0 \text{ and } a$$

$$CSCS: u = v = w = \theta_x = \phi_x = \theta_y = \phi_y = 0 \text{ at } y = 0 \text{ and } b \quad CCCC: u = v = w = \theta_x = \phi_x = \theta_y = \phi_y = 0 \text{ at } y = 0 \text{ and } b \\ u = v = w = \theta_x = \phi_x = 0 \text{ at } x = 0 \text{ and } a \quad u = v = w = \theta_x = \phi_x = \theta_y = \phi_y = 0 \text{ at } x = 0 \text{ and } a$$

#### 3.1. Convergence and validation study

Table 1 indicates that, as number of element increases—that is reducing the mesh size, graph starts converging for 3 × 3 element size. For the study, square laminated composite panel with clamped boundary condition has been used and results are tabulated for two different plate aspect ratio and number of layer combinations. Thus for the following analysis 16 elements are utilized and not changed unless stated.

In Table 2, the accuracy of the behavior for present laminated composite plate is verified by comparing the result with the available literatures. For the study, square laminated composite plate with varying aspect ratio under SSSS-I BC is considered. The results by HSDT are in close agreement with the<sup>51–54</sup> with the following material properties termed as R1,

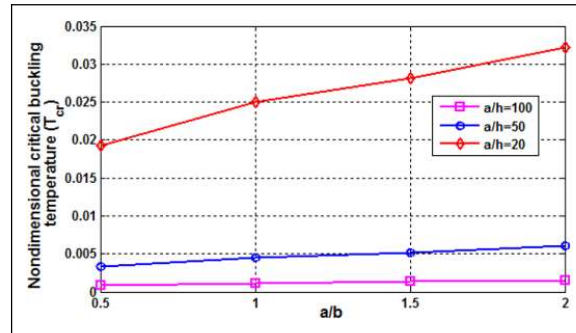
$$E_1 = 15 \times E_2, \quad G_{12} = 0.5 \times E_2, \quad G_{23} = 0.3356 \times E_2, \quad \nu_{12} = 0.3, \quad \nu_{23} = 0.49, \quad \alpha_1 = 0.015 \times \alpha_0, \quad \alpha_2 = 1 \times \alpha_0$$

Nondimensionalised critical buckling temperature (NCBT) obtained as,  $T_{cr} = \Delta T_{cr} \alpha_2$

Table 3 indicates the second validation study of simply supported square LCP with the ply orientation of [45/–45/45/–45/45/–45]. Values from Table 3 indicate nature of the variation of NCBT with the plate aspect ratio also shows comparison of result with the Lee<sup>55</sup> performed by classical laminated plate theory, first order and higher order shear

**Table 3.** Validation of NCBT with plate aspect ratio.

a/h	Lee <sup>55</sup>			Kumar and Singh <sup>49</sup>	Present
	CLT	FSDT	HSDT(A)		
5	49.3760	21.3622	21.3179	15	21.0370
10	12.3440	9.2963	9.2626	8.3	9.19062
15	5.4862	4.7885	4.7783	5.3	4.79372
20	3.0860	2.8433	2.8485	3.3	2.88414
50	0.4938	0.4874	0.4873	1.0	0.50559
80	0.1929	0.1919	0.1919	0.8	0.20030
100	0.1234	0.1230	0.1230	0.35	0.12868

**Figure 2.** Variation of NCBT with plate aspect ratio (a/b).**Table 4.** Effect of ply orientation on NCBT under thermal buckling load.

Ply Orientation	SSSS-I	CCCC	CSCS	CFCF
[90/90]	0.01537	0.03191	0.02244	0.00991
[0/0]	0.01538	0.03209	0.02515	0.00896
[0/90]	0.03117	0.05905	0.04674	0.02083
[45/45]	0.03697	0.06629	0.05353	0.02238
[0/90/0]	0.02505	0.05283	0.04021	0.01520
[90/0/90]	0.02507	0.05281	0.03818	0.01665
[45/0/45]	0.03696	0.06587	0.05213	0.02200
[45/90/45]	0.03697	0.06568	0.05208	0.02245
[45/0/45/0]	0.03364	0.05832	0.04667	0.01882
[0/90/90/0]	0.03416	0.08315	0.05111	0.02369
[90/0/0/90]	0.03420	0.08334	0.06006	0.02604
[90/0/90/0]	0.03621	0.08975	0.06724	0.03157
[30/60/60/30]	0.03657	0.07148	0.05608	0.02234
[30/60/30/60]	0.03651	0.07052	0.05608	0.02533
[30/60/-60/-30]	0.03676	0.06138	0.04039	0.01950

deformation theory. Study shows the appreciable agreement of present result with the considered literature results. The NCBT is nondimensionalised as,  $T_{cr} = \Delta T_{cr} \alpha_0 10^3$  and for the present analysis material properties utilized termed as R2,

$$E_1 = 21 \times E_0, E_2 = 1.7E_0 = E_3, G_{12} = G_{13} = 0.65E_0, G_{23} = 0.639E_0, \nu_{12} = \nu_{13} = 0.21, \nu_{23} = 0.33, E_0 = 10^9 \\ \alpha_1 = -0.21\alpha_0, \alpha_2 = 16\alpha_0$$

### 3.2. Parametric study—Thermal buckling analysis of composite laminated plate

Figure 2 shows the nature variation in NCBT with the varying plate dimensions for the layer orientation of [0/90/0], plate thickness ratio (a/h) = 100, 50 and 20, with R2 set of material properties and SSSS-I BC. Observation shows that, as aspect ratio increases, NCBT also increases. One more observation is also highlighted, that is, as thickness ratio (a/h) increases NCBT declines because of the thickness variation from thick to thin.

Effect of ply orientations and BC over NCBT is compiled in Table 4. Tabulated values proves that the thermal buckling resistance in longitudinal direction of the composite laminate is more as compared to transverse direction. Another



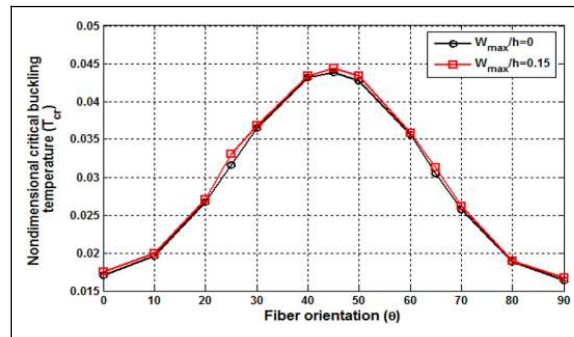


**Figure 3.** Effect of fiber orientation ( $\theta$ ) over NCBT.

**Table 5.** Variation of NCBT of LCP with plate thickness ratio and amplitude  $W_{max}/h$ .

a/h	$W_{max}/h$	Mode 1	Mode 2	Mode 3	Mode 4
5	0	0.19538	0.20497	0.21657	0.22783
	0.1	0.20057	0.22132	0.23288	0.23884
	0.2	0.20944	0.21812	0.24219	0.24479
	0.3	0.20870	0.22296	0.22907	0.23579
10	0	0.14240	0.16023	0.16601	0.18561
	0.1	0.14314	0.16626	0.16674	0.18741
	0.2	0.14518	0.16898	0.18256	0.19352
	0.3	0.14808	0.17256	0.19719	0.19859
20	0	0.07087	0.09052	0.09223	0.11735
	0.1	0.07108	0.09158	0.09242	0.11772
	0.2	0.07170	0.09293	0.09476	0.11879
	0.3	0.07267	0.09376	0.09997	0.12058
50	0	0.01694	0.02552	0.02568	0.03898
	0.1	0.01699	0.02572	0.02577	0.03905
	0.2	0.01714	0.02584	0.02649	0.03926
	0.3	0.01739	0.02605	0.02767	0.03963

observation indicates that, with cross ply laminates maximum NCBT is noticeably high as compared to single orientation, but the highest buckling resistance observed with angle ply laminates. Moreover, the highest NCBT is obtained with full clamped boundary condition whereas the lowest is at clamped free boundary condition.

Figure 3 shows the nature of variation of the NCBT with the orientation of fiber in four layered laminated composite plate of  $(\theta/-\theta/\theta/-\theta)$  with the thickness ratio of 20, SSSS-I BC and R1 set of material properties. The maximum critical buckling temperature is noticed for the ply orientation of  $40^\circ$  to  $50^\circ$ . The result also highlight the effect of the nonlinearity, that is, amplitude variation from 0 to 0.15. Moreover, as the  $W_{max}/h$  varied, the amplitude of  $T_{cr}$  increased by 0.5 to 1.5%.

Study of LCP for analyzing NCBT against square plate thickness ratio and amplitude ratio variation is shown in the Table 5. For the study R1 set of material property with ply orientation  $(45/-45/45/-45)$  under clamped BC has been considered. Post buckling analysis of LCP indicates increase of NCBT in the range of 15%, 24%, 39% and 56% as thickness ratio vary from 5 to 50, which is thick to thin. Here Mode 1 to Mode 4 denotes the first critical buckling temperature to fourth value. For the thickness ratio of 5, NCBT varies 6% for varying amplitude ratio 0 to 0.3, similarly variation is 4%, 3% for remaining thickness ratio variation with amplitude ratio. For better understanding of the thermal buckling analysis of composite laminated plate refer Figure S1 and S2 from supplementary file.

### 3.3. Parametric study—Buckling analysis of smart composite laminated plate

In section 3.2, study of LC for post buckling analysis with varying different parameter were performed with corresponding justification of the influence of individual parameter. Here, SMA wires are incorporated in the laminated composite (LC) plate to form sandwich of LC-SMA-LC configuration. Study includes the effect of temperature, plate aspect ratio, thickness ratio and BC variation over the performance of plate in terms of NCBT. For the study R3 set of material properties of LC are considered, which is stated as following.

$$E_2 = 10.3 \text{ GPa}, E_2 = E_3, E_1 = 181 \text{ GPa}, G_{12} = 7.17 \text{ GPa}, G_{12} = G_{13}, G_{23} = 6.21 \text{ GPa}, \nu_{12} = \nu_{13} = 0.28, \nu_{23} = 0.33, \alpha_0 = 10^{-6}, \alpha_1 = 0.02\alpha_0, \alpha_2 = 22.5\alpha_0$$

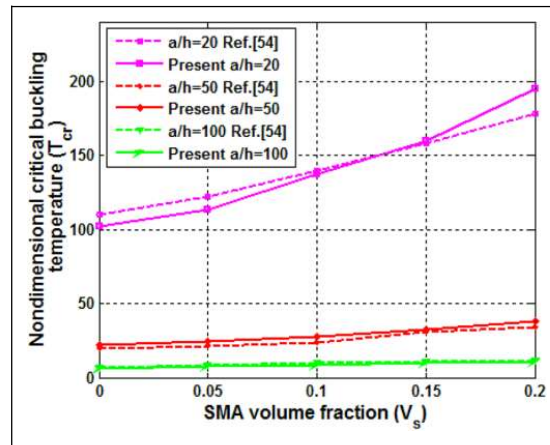


**Figure 4.** Thermal post buckling variation with SMA volume fraction.

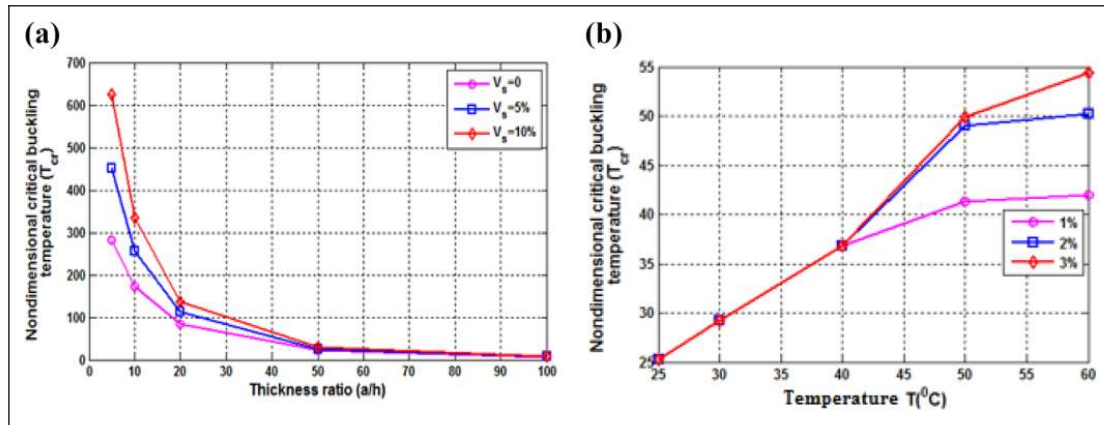


**Figure 5.** Effect of (a) plate thickness ratio with SMA volume fraction and (b) percentage strain variation over NCBT.

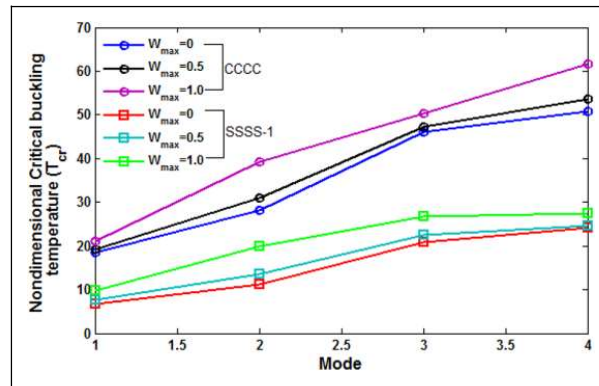
Nitinol SMA wires are utilized in the study, which has temperature dependent modulus as shown in Tawfik.<sup>50</sup>

$$E_0 = 0.1 \text{ GPa}, G = 24.86 \text{ GPa}, \alpha_1 = 10.26 \times 10^{-6}, \nu_{12} = 0.33$$

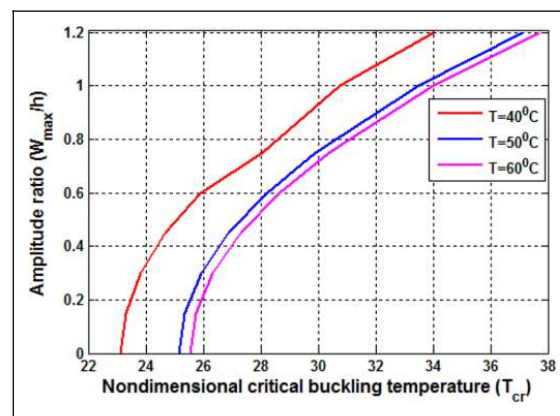
Figure 4 shows the nondimensional critical buckling temperature (NCBT) variation with the SMA volume fraction and its validation with the Kumar and Singh<sup>56</sup> performed by layerwise theory. The result indicate the same nature of variation with the available results and also shows the effect of utilization of smart composite sandwich plate under clamped boundary condition. As the SMA volume fraction is added in regular composite plate, the capacity in terms of resistance against thermal buckling  $T_{cr}$  improves.

Figure 5 (a) shows the nature of variation of NCBT with plate thickness ratio under clamped boundary condition for (0/SMA/SMA/0) orientated composite sandwich plate. In this analysis, the difference between without and with SMA layer are clearly visible. When comparing without and with SMA laminate, then it is observed that with 5% SMA volume fraction 38%, 33%, 25%, 14% and 11% more critical buckling resistance in terms of NCBT obtained at varying thickness ratios. Similarly when comparing 10% SMA laminated composite and without SMA composite laminate, then corresponding variation in NCBT will be 28%, 24%, 18%, and 12%. So with minor incorporation of SMA wires, and utilizing its shape memory behavior, the critical buckling resistance of the structure can get improved. The effect of induced pre-strains with increasing temperature over NCBT for sandwich composite clamped plate having thickness ratio of 50 is shown in Figure 5 (b). During heating cycle, pre-strain is induced to increase thermal buckling resistance for the plate. From Tawfik,<sup>50</sup> it is observed that, till 40°C elastic modulus and recovery stress remains constant, but above this temperature, these values starts varying. So from 50°C, NCBT increases approximately by 16% for 2% strain compared to 1% strain and 2–8% for 3% strain as compared to 2% strain.

Figure 6 shows the first four buckling modes for clamped and simply supported BC for the amplitude ratio of 0, 0.5 and 1 for four layered (45/SMA/SMA/45) composite sandwich plate with thickness ratio of 50. More resistance against buckling is observed in clamped BC as compared to SSSS-1. The difference of 19% and 11% are observed for



**Figure 6.** Variation in NCBT with the amplitude ratio under different BC.



**Figure 7.** Effect of temperature and amplitude ratio variation over NCBT.

amplitude ratio of 0 to 0.5 and 0.5 to 1 under mode 1, and similarly for clamped condition that difference is 3% and 9–10% respectively.

The nature of variation of NCBT with the amplitude ratio under different temperature variation is shown in Figure 7, for the (45/SMA/SMA/45) clamped sandwich layup with the plate thickness ratio of 50 and  $\varepsilon_r = 1\%$ . It can be observed that for the different temperature variation, with variation of amplitude ratio from 0 to 1.2, NCBT increases by 32%. Also, as temperature increases from 40°C to 50°C, then NCBT increases by 8%, whereas, during temperature variation from 50°C to 60°C, it increases by 2%. Thus, the study highlights effect of temperature variation over buckling resistance in structure with the SMA reinforcement. Supplementary inferences are presented in Figure S3, S4 and S5 from supplementary file to elaborate the buckling analysis of smart composite laminated plate.

### 3.4. Effect of shape memory polymers on buckling behavior of SMA hybrid composite

The dynamic variation in SMPC material parameter exists in the vicinity of glass transition temperature ( $T_g$ ), which shows the longitudinal, transverse and shear behavior is stable before and after this range as given in Figure 8. Figure 8 (a) has been plotted from Eq. 1 and The trajectory follows the similar behavior of SMP as indicated in previous results.<sup>45</sup>

SMA reinforced laminates have dynamic property in the austenite and martensite region of alloy whereas dynamic property of SMP is governed by its glass transition region. Longitudinal, transverse and shear modulus of carbon is considered as 230 GPa, 8.2 GPa and 27.3 GPa respectively.<sup>57</sup> The laminate behaves with dual dynamic property because of the combined property of SMP and SMA. Figure 9 (a) indicates combined behavior of unidirectional SMA reinforced SMP sandwich composite laminated plates with  $a/h = 15$  and edges clamped at ends. The laminate has 10% SMA fiber in second and third layers whereas in the first and fourth layers 10% carbon fiber is reinforced. Tawfik<sup>50</sup> indicates that, in a region 0°C to 30°C, temperature dependent elastic modulus of SMA fiber doesn't show much variation as well as recovery stresses remains zero during same interval. But at the same, dynamic variation in elastic modulus of SMPC is observed. Figure 9 (a and b) highlights the abrupt decline which is due to the volatile material behavior of SMP matrix and SMA fiber reinforcements in the similar temperature span. It can be observed that instantaneous drop is regulated by

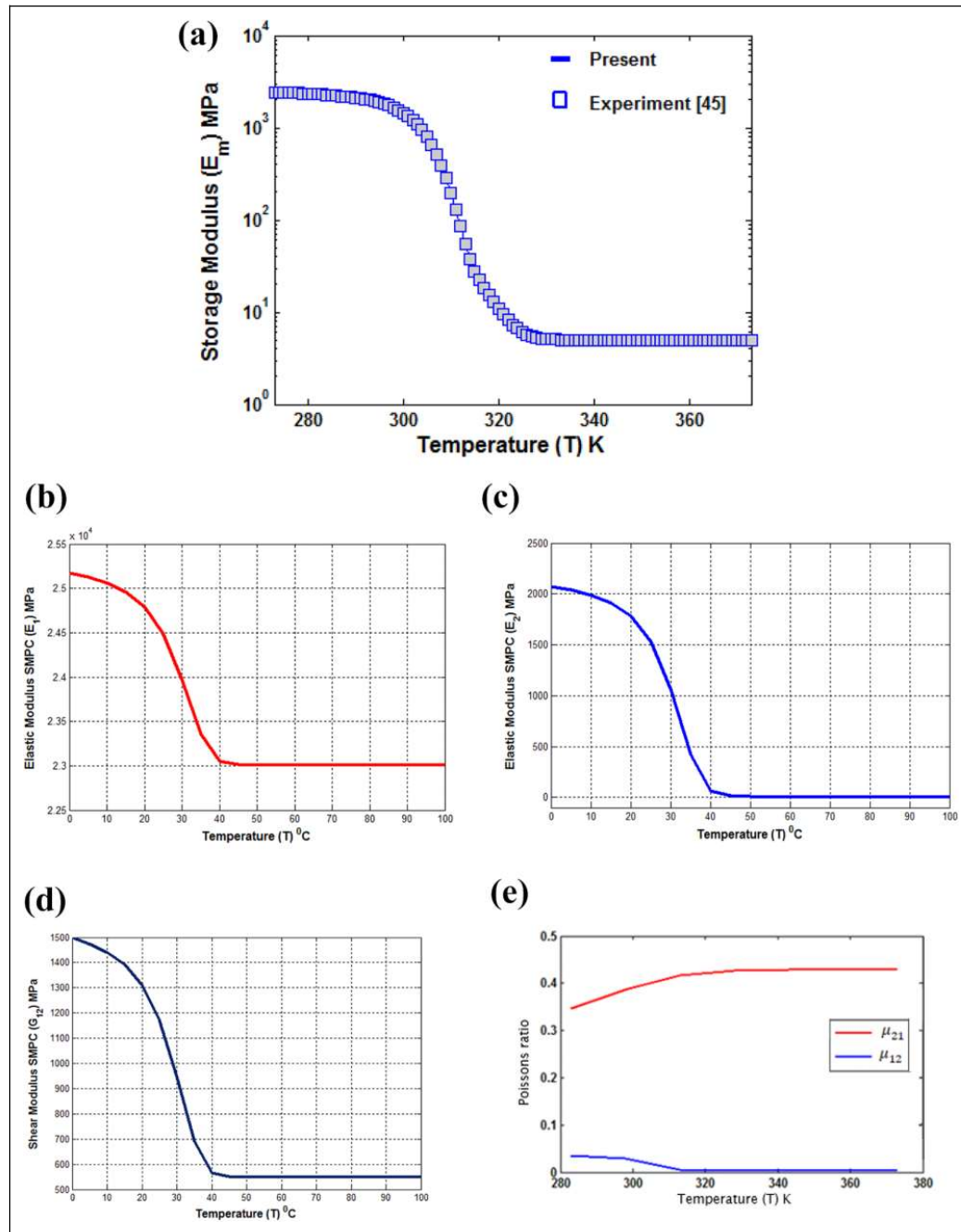
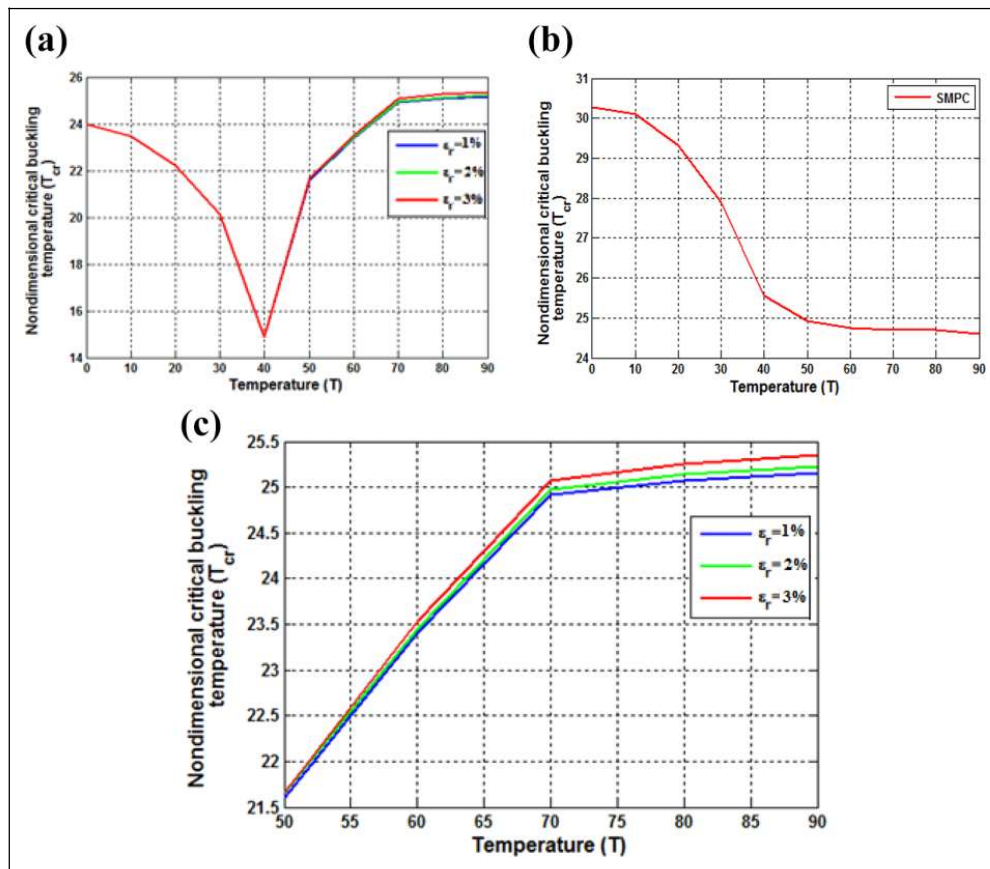


**Figure 8.** Influence of variation of temperature on modulus: (a) of SMP  $E_m$  (b) longitudinal, (c) transverse (d) shear modulus and (e) Poisson's ratio of SMPC.

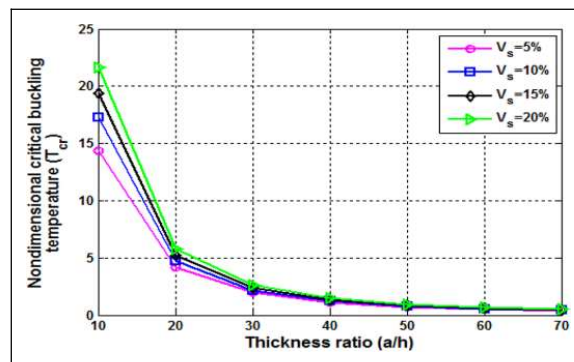
modulus of SMP matrix, which regulates the profile of buckling load. After  $40^\circ\text{C}$ , in accordance with Tawfik<sup>50</sup> the elastic modulus of SMA fiber instantaneously increases, which regulates sudden rise in buckling resistance of SMA reinforced SMPC beam. Figure 9 (a and b) indicates conclusive comparison of positive effect of combined shape memory properties of SMA and SMP on buckling resistance of material at elevated temperature. This is primarily due to the recovery stresses of SMA generated at elevated temperatures which enhances the stability of material as compared to normal SMPC or laminated composite structure. Figure 9 (c) shows the elaborated part of Figure 9 (a). Figure shows that with the strain rate and temperature variation, the NCBL also increases.

Figure 10 shows the analysis of SMA embedded SMPC sandwich plate with the varying volume fraction of the SMA for the (0/SMA/SMA/0) plate under SSSS-1 BC. For the presented SMA embedded SMPC sandwich plate, whenever the SMA volume fraction increases, the NCBT also increases by 17%, 12% and 11% for the Vs of 5% to 20%.





**Figure 9.** Variation in NCBL with the (a) combined influence of SMPC and SMA (b) SMPC only and (c) enlarge view of with strain rate and temperature.



**Figure 10.** Variation in NCBT with the SMA volume fraction.

#### 4. Conclusions and future scope

Under induced uniform thermal loading, non-linear thermal post-buckling analysis of laminated composite plate, smart sandwich composite plate and for first time the combined effect of SMA and SMP is analyzed using higher order shear deformation theory and von Karman kinematics. The following observations are listed down during the study,

1. The thermal buckling resistance in longitudinal direction of the composite laminate is higher than that in transverse direction. Also, with angle ply laminate, the highest thermal buckling resistance is observed among all the considered plate configurations.
2. For four layered lamination whenever ply orientations varies from  $0^\circ$  to  $90^\circ$ , the maximum NCBT were noted between  $40^\circ - 50^\circ$  range and also results elaborate effect of minor amplitude ratio application over NCBT increased by 05 to 1.5%.

3. NCBT is minimum at simply supported BC whereas it is maximum with clamped BC.
4. Analysis indicates that, with minor incorporation of SMA wires, and utilizing its shape memory behavior, the critical buckling resistance of the structure can be appreciably improved.
5. With increasing prestrain induced rate in SMA, the NCBT can also be enhanced, as the result clearly differentiate the effect of increasing SMA layers over thermal buckling analysis.
6. When analyzing effect of temperature and amplitude ratio variation over NCBT, as temperature increases from 40<sup>0</sup> C to 50<sup>0</sup> C, then NCBT increases by 8%, whereas, during temperature variation from 50<sup>0</sup> C to 60<sup>0</sup> C, it increases by 2%.
7. Due to the combined effect of the SMA-SMP, corresponding smart sandwich indicate improved buckling resistance for the wide range of temperature, except for the break-point observed in the analysis.

For the suggested model and method, first time the combined effect of SMA embedded SMPC has been studied from buckling point of view. Still there are plenty of opportunities available for extending the study, such as analyzing the effect of the nonlinear and nonuniform temperature variation effect on thermal buckling and vibration of smart composite panels. As great variety of fibers are available, so it could be possible to perform series test, to prove accuracy and validity of the model. For thermo-electro-mechanical finite deformation for smart materials, multi configuration theory can be utilized.


### Declaration of conflicting interests

The author(s) declared no potential conflicts of interest with respect to the research, authorship, and/or publication of this article.

### Funding

The author(s) received no financial support for the research, authorship, and/or publication of this article.

### ORCID iD

Achchhe Lal  <https://orcid.org/0000-0001-7496-2112>

### Supplemental material

Supplemental material for this article is available online.

### References

1. Lagoudas DC. *Shape memory alloys: modeling and engineering applications*. Berlin: Springer Science & Business Media, 2008.
2. Asadi H, Akbarzadeh AH and Wang Q. Nonlinear thermo-inertial instability of functionally graded shape memory alloy sandwich plates. *Compos Struct* 2015; 120: 496–508.
3. Khalili SMR, Botshekanan DM, Carrera E, et al. Non-linear dynamic analysis of a sandwich beam with pseudoelastic SMA hybrid composite faces based on higher order finite element theory. *Compos Struct* 2013; 96: 243–255.
4. Frostig Y and Thomsen OT. High-order free vibration of sandwich panels with a flexible core. *Int J Solids Struct* 2004; 41: 1697–1724.
5. Ko WL. Predictions of thermal buckling strengths of hypersonic aircraft sandwich panels using minimum potential energy and finite element methods. *NASA Technical Memorandum* May 1995; 4643: 1–54.
6. Sadighi M and Pouriayevali H. Quasi-static and low-velocity impact response of fully backed or simply supported sandwich beams. *J Sand Struct Mater* 2008; 10: 499–524.
7. Afshin M, Sadighi M and Shakeri M. Static analysis of cylindrical sandwich panels with a flexible core and laminated composite face sheets. *J Compos Mater* 2010; 44: 1455–1476.
8. Mansouri MH and Shariyat M. Thermal buckling predictions of three types of high-order theories for the heterogeneous orthotropic plates, using the new version of DQM. *Compos Struct* 2014; 113: 40–55.
9. Li ZM. Thermal postbuckling behavior of 3D braided beams with initial geometric imperfection under different type temperature distributions. *Compos Struct* 2014; 108: 924–936.
10. Lee JJ and Choi S. Thermal buckling and postbuckling analysis of a laminated composite beam with embedded SMA actuators. *Compos Struct* 1999; 47: 695–703.
11. Asadi H, Bodaghi M, Shakeri M, et al. On the free vibration of thermally pre/post-buckled shear deformable SMA hybrid composite beams. *Aerospace Sci Technol* 2013; 31: 73–86.
12. Asadi H, Kiani Y, Shakeri M, et al. Exact solution for nonlinear thermal stability of hybrid laminated composite Timoshenko beams reinforced with SMA fibers. *Compos Struct* 2014; 108: 811–822.
13. Girish J and Ramachandra LS. Thermal postbuckled vibrations of symmetrically laminated composite plates with initial geometric imperfections. *J Sound Vibrat* 2005; 282: 1137–1153.



14. Singh G, Rao GV and Lyengar NGR. Large amplitude free vibration of simply supported antisymmetric cross-ply plates. *AIAA J* 1991; 29: 784–790.
15. Reddy JN and Chao WC. Nonlinear oscillations of laminated, anisotropic, rectangular plates. *J Appl Mech* 1982; 49: 396–402.
16. Khdeir AA. Thermal buckling of cross-ply laminated composite beams. *Acta Mechanica* 2001; 149: 201–213.
17. Aydogdu M. Thermal buckling analysis of cross-ply laminated composite beams with general boundary conditions. *Compos Sci Technol* 2007; 67: 1096–1104.
18. Vosoughi AR, Malekzadeh P, Banan MAR, et al. Thermal buckling and postbuckling of laminated composite beams with temperature-dependent properties. *Int J Non-Linear Mech* 2012; 47: 96–102.
19. Rogers C and Barker D. Experimental studies of active strain energy tuning of adaptive composites. In: *31st structures, structural dynamics and materials conference*, American Institute of Aeronautics and Astronautics, 2–4 April 1990.
20. Baz A, Poh S, Ro J, et al. Active control of nitinol-reinforced composite beam. In: Tzou HS and Anderson GL (eds) *Intelligent structural systems*. Dordrecht: Springer Netherlands, 1992, pp. 169–212.
21. Khalili SMR and Akbari T. Study on the effective parameter of buckling behavior of cylindrical composite shells with embedded SMA wires. *J Reinforc Plast Compos* 2019; 38(16): 737–748.
22. Choi S, Lee JJ, Seo DC, et al. The active buckling control of laminated composite beams with embedded shape memory alloy wires. *Compos Struct* 1999; 47: 679–686.
23. Birman V. Stability of functionally graded shape memory alloy sandwich panels. *Smart Mater Struct* 1997; 6: 278–286.
24. Lee HJ, Lee JJ and Huh JS. A simulation study on the thermal buckling behavior of laminated composite shells with embedded shape memory alloy (SMA) wires. *Compos Struct* 1999; 47: 463–469.
25. Park JS, Kim JH and Moon SH. Vibration of thermally post-buckled composite plates embedded with shape memory alloy fibers. *Compos Struct* 2004; 63: 179–188.
26. Li SR, Yu WS and Batra RC. Free vibration of thermally pre/post-buckled circular thin plates embedded with shape memory alloy fibers. *J Ther Stress* 2010; 33: 79–96.
27. Shiau LC, Kuo SY and Chang SY. Free vibration of buckled SMA reinforced composite laminates. *Compos Struct* 2011; 93: 2678–2684.
28. Parhi A and Singh BN. Nonlinear free vibration analysis of shape memory alloy embedded laminated composite shell panel. *Mech Adv Mater Struct* 2017; 24: 713–724.
29. Nejati M, Ghasemi-Ghalebahman A, Soltanmaleki A, et al. Thermal vibration analysis of SMA hybrid composite double curved sandwich panels. *Compos Struct* 2019; 224(1): 1–11.
30. Salim M, Bodaghi M, Kamarian S, et al. Free vibration analysis and design optimization of SMA/graphite/epoxy composite shells in thermal environments. *Latin Am J Solid Struct* 2018; 15. DOI: 10.1590/1679-78253070.
31. Panda SK and Singh BN. Thermal post-buckling behaviour of laminated composite cylindrical/hyperboloid shallow shell panel using nonlinear finite element method. *Compos Struct* 2009; 91: 366–374.
32. Panda SK and Singh BN. Nonlinear finite element analysis of thermal post-buckling vibration of laminated composite shell panel embedded with SMA fibre. *Aerospace Sci Technol* 2013; 29: 47–57.
33. Xia XK and Shen HS. Vibration of postbuckled FGM hybrid laminated plates in thermal environment. *Eng Struct* 2008; 30: 2420–2435.
34. Tawfik M, Ro JJ and Mei C. Thermal post-buckling and aeroelastic behaviour of shape memory alloy reinforced plates. *Smart Mater Struct* 2002; 11: 297–307.
35. Zhong ZW, Chen RR, Mei C, et al. Buckling and post-buckling of shape memory alloy fiber-reinforced composite plates. In: *Symposium on buckling and post-buckling of composite structure*, ASME AD, 1994, vol. 41/293, pp. 115–132.
36. Lee HJ and Lee JJ. A numerical analysis of the buckling and post-buckling behavior of laminated composite shells with embedded shape memory alloy wire actuators. *J Smart Mater Struct* 2000; 9: 780–787.
37. Kheirikhah MM and Khosravi P. Buckling and free vibration analyses of composite sandwich plates reinforced by shape-memory alloy wires. *J Brazil Soci Mech Sci Eng* 2018; 40: 515.
38. Samadpour M, Sadighi M, Shakeri M, et al. Vibration analysis of thermally buckled SMA hybrid composite sandwich plate. *Compos Struct* 2015; 119: 251–263.
39. Bayat Y and Ekhteraei TH. Exact solution of thermal buckling and post buckling of composite and SMA hybrid composite beam by layerwise theory. *Aerospace Sci Technol* 2017; 67: 484–494.
40. Asadi H, Eynbeygi M and Wang Q. Nonlinear thermal stability of geometrically imperfect shape memory alloy hybrid laminated composite plates. *Smart Mater Struct* 2014; 23: 075012.
41. Kabir MZ and Tehran BT. Closed-form solution for thermal, mechanical, and thermo-mechanical buckling and post-buckling of SMA composite plates. *Compos Struct* 2017; 168: 535–548.
42. Karimiasl M, Ebrahimi F and Akgöz B. Buckling and post-buckling responses of smart doubly curved composite shallow shells embedded in SMA fiber under hygro-thermal loading. *Compos Struct* 2019; 223: 110988.
43. Mahieux CA and Reifsnider KL. Property modeling across transition temperatures in polymers: a robust stiffness–temperature model. *Polymer* 2001; 42: 3281–3291.
44. Westbrook KK, Kao PH, Castro F, et al. A 3D finite deformation constitutive model for amorphous shape memory polymers: a multi-branch modeling approach for nonequilibrium relaxation processes. *Mech Mater* 2011; 43: 853–869.

45. Gu J, Leng J, Sun H, et al. Thermomechanical constitutive modeling of fiber reinforced shape memory polymer composites based on thermodynamics with internal state variables. *Mech Mater* 2019; 130: 9–19.
46. Qi HJ, Nguyen TD, Castro F, et al. Finite deformation thermo-mechanical behavior of thermally induced shape memory polymers. *J Mech Phys Solid* 2008; 56: 1730–1751.
47. Jagtap KR, Lal A and Singh BN. Thermomechanical elastic post-buckling of functionally graded materials plate with random system properties. *Int J Computat Method Eng Sci Mech* 2013; 14: 175–194.
48. Lal A, Singh BN and Kale S. Stochastic post buckling analysis of laminated composite cylindrical shell panel subjected to hygro-thermo-mechanical loading. *Compos Struct* 2011; 93: 1187–1200.
49. Kumar SK and Singh BN. Thermal buckling analysis of SMA fiber-reinforced composite plates using layerwise model. *J Aerosp Eng* 2009; 22(4): 342–353.
50. Tawfik M. *Suppression of post-buckling deflection and panel-flutter using shape memory alloy*. MSc thesis, Aerospace Department, Old Dominion University, Norfolk VA, 1999.
51. Matsunaga H. Thermal buckling of cross-ply laminated composite and sandwich plates according to a global higher-order deformation theory. *Compos Struct* 2005; 68: 439–454.
52. Noor AK and Burton WS. Three-dimensional solutions for thermal buckling of multilayered anisotropic plates. *J Eng Mech* 1992; 118: 683–701.
53. Singh S, Singh J and Shukla K. Buckling of laminated composite plates subjected to mechanical and thermal loads using meshless collocations. *J Mech Sci Technol* 2013; 27: 327–336.
54. Mirzaei M and Kiani Y. Thermal buckling of temperature dependent FG-CNT reinforced composite plates. *Meccanica* 2016; 51: 2185–2201.
55. Lee J. Thermally induced buckling of laminated composites by a layerwise theory. *Comput Struct* 1997; 65(6): 917–922.
56. Kumar CN and Singh BN. Thermal buckling and post-buckling of laminated composite plates with SMA fibers using layerwise theory. *Int J Comput Method Eng Sci Mech* 2009; 10(6): 423–429.
57. Shen GL, Hu G and Liu B. *Mechanics of composite materials*. Beijing, China: Science and Technology, 2006.

## Appendix

$$L = \begin{bmatrix} \frac{\partial}{\partial x} & 0 & 0 & 0 & 0 & 0 & 0 \\ 0 & \frac{\partial}{\partial y} & 0 & 0 & 0 & 0 & 0 \\ \frac{\partial}{\partial y} & \frac{\partial}{\partial x} & 0 & 0 & 0 & 0 & 0 \\ 0 & 0 & 0 & 0 & 0 & 0 & C_1 \frac{\partial}{\partial x} \\ 0 & 0 & 0 & 0 & 0 & C_1 \frac{\partial}{\partial y} & 0 \\ 0 & 0 & 0 & 0 & 0 & C_1 \frac{\partial}{\partial y} & C_1 \frac{\partial}{\partial x} \\ 0 & 0 & 0 & 0 & -C_4 \frac{\partial}{\partial x} & 0 & -C_2 \frac{\partial}{\partial x} \\ 0 & 0 & 0 & -C_4 \frac{\partial}{\partial y} & 0 & -C_2 \frac{\partial}{\partial y} & 0 \\ 0 & 0 & 0 & -C_4 \frac{\partial}{\partial x} & -C_4 \frac{\partial}{\partial y} & -C_2 \frac{\partial}{\partial x} & -C_2 \frac{\partial}{\partial y} \\ 0 & 0 & C_1 \frac{\partial}{\partial y} & 0 & 0 & C_1 & 0 \\ 0 & 0 & C_1 \frac{\partial}{\partial x} & 0 & 0 & 0 & C_1 \\ 0 & 0 & 0 & -3C_4 & 0 & -3C_2 & 0 \\ 0 & 0 & 0 & 0 & -3C_4 & 0 & -3C_2 \end{bmatrix} \quad (A1)$$

$$[\bar{Q}]_m = \begin{bmatrix} \bar{Q}_{11m} & \bar{Q}_{12m} & \bar{Q}_{13m} & 0 & 0 \\ \bar{Q}_{12m} & \bar{Q}_{22m} & \bar{Q}_{23m} & 0 & 0 \\ \bar{Q}_{13m} & \bar{Q}_{23m} & \bar{Q}_{33m} & 0 & 0 \\ 0 & 0 & 0 & \bar{Q}_{44m} & 0 \\ 0 & 0 & 0 & 0 & \bar{Q}_{55m} \end{bmatrix} \quad \text{and} \quad [\bar{Q}] = \begin{bmatrix} \bar{Q}_{11} & \bar{Q}_{12} & \bar{Q}_{13} & 0 & 0 \\ \bar{Q}_{12} & \bar{Q}_{22} & \bar{Q}_{23} & 0 & 0 \\ \bar{Q}_{13} & \bar{Q}_{23} & \bar{Q}_{33} & 0 & 0 \\ 0 & 0 & 0 & \bar{Q}_{44} & 0 \\ 0 & 0 & 0 & 0 & \bar{Q}_{55} \end{bmatrix} \quad (\text{A2})$$

$$\bar{Q}_{11m} = \bar{Q}_{22m} = \frac{Ec}{1 - \nu_m^2}, \quad \bar{Q}_{12m} = \frac{\nu_m Ec}{1 - \nu_m^2}, \quad \bar{Q}_{44m} = \bar{Q}_{55m} = \frac{Ec}{2(1 + \nu_m)}$$

$$D = \sum_{k=1}^{NL} \int_{z_{k-1}}^{z_k} [T] [\bar{Q}_{ij}] [T] dz = \begin{bmatrix} [A_1] & [B] & [E] & 0 & 0 \\ [B] & [C_1] & [F_1] & 0 & 0 \\ [E] & [F_1] & [H] & 0 & 0 \\ 0 & 0 & 0 & [A_2] & [C_2] \\ 0 & 0 & 0 & [C_2] & [F_2] \end{bmatrix} \quad (\text{A3})$$

$$D_1 = \begin{bmatrix} A_1 & 0 \\ B & 0 \\ E & 0 \\ 0 & A_2 \\ 0 & C_2 \end{bmatrix}; \quad D_2 = \begin{bmatrix} A_1 & B & E & 0 & 0 \\ 0 & 0 & 0 & A_2 & C_2 \end{bmatrix}; \quad D_3 = \begin{bmatrix} A_1 & 0 \\ 0 & A_2 \end{bmatrix} \quad (\text{A4})$$